Available online at www.sciencedirect.com
ScienceDirect
Journal of the European Ceramic Society 30 (2010) 289–293
www.elsevier.com/locate/jeurceramsoc

Size effects in Fe^{3+}-doped $PbTiO_3$ nanocrystals—Formation and orientation of $(Fe'_{Ti}-V_O^{\bullet\bullet})^{\bullet}$ defect-dipoles

Emre Erdem [a], Kamil Kiraz [b], Mehmet Somer [b], Rüdiger-A. Eichel [a,*]

[a] *Institut für Physikalische Chemie I, Universität Freiburg, Albertstr. 21, D-79104 Freiburg, Germany*
[b] *Koc University, Department of Chemistry, Rumelifeneri Yolu, Sariyer, 34450 Istanbul Turkey*

Received 19 September 2008; received in revised form 15 April 2009; accepted 26 April 2009
Available online 31 May 2009

Abstract

A set of Fe^{3+}-modified $PbTiO_3$ nanopowders has been synthesized according to the combined polymerization and pyrolysis (CPP) route of metallorganic precursors [Erdem E, Böttcher R, Semmelhack H-C, Gläsel H-J, Hartmann E, Hirsch D. Preparation of lead titanate ultrafine powders from combined polymerisation and pyrolysis route. *J. Mater. Sci.* 2003;**38**:3211–7] with subsequent calcination at various temperatures. X-ray diffraction verifies the formation of a $PbTiO_3$ perovskitic phase and Raman-spectroscopy proves the existence of ferroelectricity.

Furthermore, the prevailing defect structure has been investigated by means of electron paramagnetic resonance (EPR) spectroscopy. The EPR results clearly indicate marked size effects by approaching to the critical grain size ($d_{crit} < 12$ nm) at which a size-driven tetragonal-to-cubic phase transition is observed at room temperature. As a function of mean grain size, either $(Fe'_{Ti}-V_O^{\bullet\bullet})^{\bullet}$ defect dipoles or 'isolated' defects (Fe'_{Ti}, $V_O^{\bullet\bullet}$) are formed. These results are analyzed in terms of a *core–shell model*. Accordingly, the obtained Fe^{3+}-modified $PbTiO_3$ nanoparticles consist of a ferroelectric core, a distorted interface region, and a cubic dead layer which is paraelectric.

Keywords: Size effects; Ferroelectric-to-paraelectric phase transition; Critical size; Lead titanate ferroelectrics; Iron doping; Oxygen vacancies; Defect dipoles

1. Introduction

Owing to its intrinsic high tetragonality and high Curie temperature T_C, lead titanate ($PbTiO_3$, PT) is a promising candidate for nano-technological ferroelectric devices. More general, ferroelectricity is a collective phenomenon involving the cooperation of polar distortions through both, short-range chemical and long-range dipolar interactions. As a consequence, the ferroelectric transition is strongly affected or even suppressed for small particle sizes (nano-structures) or confined geometries (thin films).[1] As a function of reduced size, the long-range forces become weaker, and *vice-versa* the short-range forces become dominand. Consequently, below a critical size d_{crit} a size-driven para-to-ferroelectric phase transition is observed. However, the exact size of d_{crit} for different systems is still controversially discussed.[2,3,4,5] Typically, for thin-films critical sizes well below 10 nm are reported.[6,7,8]

A still open question, however, is how size or confined geometry impacts the defect structure, such as the formation or orientation of acceptor–oxygen vacancy defect dipoles.[9,10] In 'bulk' ferroelectrics, it was recently reported that acceptor-type centers form defect dipoles with charge-compensating oxygen vacancies, such as $(Fe'_{Zr,Ti}-V_O^{\bullet\bullet})^{\bullet}$ [11,12] or $(Cu''_{Zr,Ti}-V_O^{\bullet\bullet})^{\times}$ [13,14] in $Pb[Zr_xTi_{1-x}]O_3$ (PZT). By doping over the solubility limit, which typically is in the order of a few percent, secondary magnetic phases may be formed.[15] On the other hand, donor-type centers tend to form rather 'isolated' functional centers where the excess charge in form of lead vacancies (V''_{Pb}) is compensated in distant coordination spheres.[16] Concerning the $(Fe'_{Zr,Ti}-V_O^{\bullet\bullet})^{\bullet}$ defect dipoles, their orientation with respect to the one of the spontaneous polarization is a function of crystal symmetry and lattice distortion.[19,17,18] For this reason a marked effect on the formation and orientation of $(Fe'_{Ti}-V_O^{\bullet\bullet})^{\bullet}$ defect dipoles is expected for $PbTiO_3$ nanocrystals. Furthermore, upon the application of a suitable electric field the defect dipoles reorient along the direction of spontaneous polarization.[20]

* Corresponding author. Fax: +49 761 2036222.
E-mail address: r.eichel@physchem.uni-freiburg.de (R.-A. Eichel).

0955-2219/$ – see front matter © 2009 Elsevier Ltd. All rights reserved.
doi:10.1016/j.jeurceramsoc.2009.04.034

On the other hand, it is known that the Curie temperature for 'bulk' ferroelectric systems may be altered by doping with different transition-metal ions.[21] Consequently, the critical size may also be impacted. For Cr^{3+}-modified $PbTiO_3$ nanocrystals, a critical size of $d_{crit} = 6$ nm has recently been reported.[22] In this work, we therefore aim to synthesize and systematically study of the interplay between grain size and characteristics of $(Fe'_{Zr,Ti}{-}V_O^{\bullet\bullet})^{\bullet}$ defect dipoles in Fe^{3+}-modified $PbTiO_3$ nanocrystals.

2. Experimental

2.1. Synthesis

The Fe^{3+}-modified $PbTiO_3$ nanocrystals were prepared by the recently introduced combined polymerization and pyrolysis (CPP) route of metallorganic precursors,[23] which can be applied for preparing doped perovskitic ultra-fine powders.[24,25,22] The main advantages of CPP route are the easy incorporation of transition-metal ions, the requirement of comparatively low crystallization temperatures (below 400 °C) and the simplicity of controlling the particle size by adjusting the preparation temperature. This method gives good surface morphology, phase purity and non-agglomerated nanoparticles.[23] The drawback of this route is, however, that no $PbTiO_3$ nanoparticles with mean grain size below 30 nm can be synthesized. In order to circumvent this shortcoming, short-time soft milling of a parent nanopowder obtained from a tempering route at medium temperature has been subsequently performed, giving particles with mean grain size below 10 nm. With the very low mechanical energy requirement it is possible to reduce the particle sizes below 10 nm.[27]

In detail, the CPP route is based on a route for synthesizing of nanoferrites[26] and involves the following two stages: (i) preparation of metallo-organic precursor and (ii) polymerisation and pyrolysis. The chemicals used in these processes are lead(II) oxide (PbO)—Aldrich, titanium(IV) isopropoxide ($Ti(O{-}C_3H_7)_4$)—Aldrich, and methacrylic acid ($CH_2{=}C(CH_3){-}COOH$)—Aldrich. Due to the synthesis conditions (open system), a certain loss of the lead component had to be taken into account, and for a corresponding compensation 10 percent surplus of PbO was used with respect to the stoichiometry. Iron(III) acetylacetonate ($Fe(CH_3COCH{=}C(O^{\bullet})CH_3)_3$)—Aldrich, was employed as dopant because it does not only contain Fe^{3+} ions but is also readily soluble in chloroform.

(I) Metallo-organic precursor: Lead titanyl methacrylate was obtained as a monomeric metallo-organic precursor from lead oxide, titanium(IV) isopropoxide and methacrylic acid in boiling pure chloroform ($CHCl_3$) (magnetic stirring, 3 h, 150 °C) by four reactions as described below. A stabiliser (4-methoxyphenol) was added to the solution to avoid polymerisation of methacrylic acid during the heating. Individual formation reactions of lead methacrylate and titanium propoxide methacrylate from PbO and $Ti(O{-}C_3H_7)_4$can be written as follows:

$$PbO + 2CH_2{=}C(CH_3){-}COOH \rightarrow Pb(OOC{-}C(CH_3{=}CH_2))_2 + H_2O. \quad (1)$$

$$Ti(O{-}C_3H_7)_4 + 2CH_2{=}C(CH_3{-}COOH \rightarrow Ti(O{-}C_3H_7)_2)((OOC{-}C(CH_3){=}CH_2)_2) + 2C_3H_7OH. \quad (2)$$

In presence of both PbO and $Ti(O{-}C_3H_7)_4$ in methacrylic acid, the reaction product will be a mixture of (1) and (2), thus:

$$PbO + Ti(O{-}C_3H_7)_4 + 4CH_2{=}C(CH_3){-}COOH \rightarrow PbTi(O{-}C_3H_7)_2(OOC{-}C(CH_3){=}CH_2)_4 + H_2O + 2C_3H_7OH. \quad (3)$$

The final organometallic precursor (4) can be obtained by addition of water while refluxing. This step is necessary to complete the partial ligand exchange reaction of titanium in (2).

$$PbTi(O{-}C_3H_7)_2(OOC{-}C(CH_3){=}CH_2)_4 + H_2O \rightarrow PbTiO(OO{-}C(CH_3){=}CH_2)_4 + 2C_3H_7OH. \quad (4)$$

The solvent used in (1)–(4) was chloroform (boiling point: 62 °C) which was removed by rotary evaporation. The solid precursor was placed in an oven for 2 days at 70 °C for drying and grinded to fine powder for further use.

(II) Combined polymerisation and pyrolysis: This process is rather complex and may be described by three reaction steps:

$$nPbTiO(OOC{-}C(CH_3){=}CH_2)_4 \rightarrow (PbTiO(OOC{-}C(CH_3){-}CH_2)_4)_n \quad (5)$$

$$(PbTiO(OOC{-}C(CH_3){-}CH_2)_4)_n \rightarrow PbCO_3 + TiO_2 + C + \text{volatiles} \quad (6)$$

$$PbCO_3 + TiO_2 \rightarrow PbTiO_3 + CO_3. \quad (7)$$

The solid state polymerisation (5) and the concomitant pyrolysis (6) proceed simultaneously at temperatures above 165 °C. Nucleation (6) and growth of $PbTiO_3$ particles (7) start at about 385 °C, where the temperature and the reaction atmosphere determine the resulting particle size. In Fig. 1 the corresponding calcination scheme for the control of the resulting mean particle size of the $PbTiO_3$ nanaocrystals. Typically, the samples were annealed for 6 h at the target temeprature and hereby an increase of the particles size was observed when the annealing temperature was elevated.

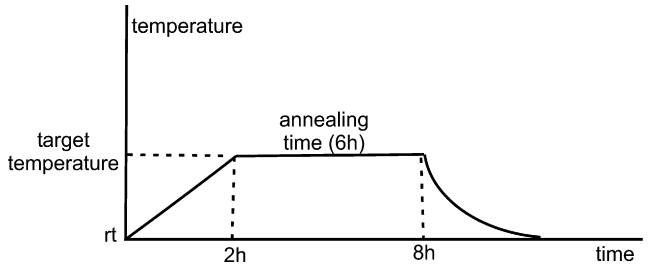

Fig. 1. Schematic representation of the calcination scheme for the CPP route in order to control the resulting particle size.

2.2. Characterization

X-ray diffraction (XRD) measurements were carried out at room temperature with a powder diffractometer Huber G670 equipped with a germanium monochromator, using Cu-K_α radiation. The particle size was determined using Scherrer's equation $D = (k\lambda/\beta\cos(\theta))$ where D is the mean grain size, k the Scherrer's constant ($k = 0.9$ for FWHM), λ the X-ray wavelength, β the FWHM of a diffraction peak, and θ the diffraction angle.

The FT-Raman spectra were recorded using an Bruker RFS 100 spectrometer with Nd:YAG laser as excitation source at a power level of up to 30 mW.

The X-band (9.5 GHz) continuous-wave (cw) EPR measurements were performed using an ESP 300E spectrometer (Bruker), equipped with a rectangular TE_{112} resonator. All EPR measurements performed at ambient temperature.

For numerical spectrum analysis of the EPR data, the free trivalent iron ion is considered as possessing five unpaired electrons in the $3d$ shell ($3d^5$) with a high-spin $^6S_{5/2}$ ground state ($S = 5/2$). The crystal field originating from the nearest neighbor oxygen ions (and possibly oxygen vacancies) lifts the Fe^{3+} spin degeneracy resulting in three Kramer's doublets, whose degeneracy in turn is lifted by an external magnetic field. Neglecting hyperfine interaction, as the only isotope with non-vanishing nuclear spin ^{57}Fe is present in only 2.15% natural abundance, an approximate spin Hamiltonian for these high-spin system can be written as

$$\mathcal{H} = g_{\mathrm{iso}}\beta_e \mathbf{B}_0 \cdot \mathbf{S} + \sum_{k}^{-k\le q\le k} B_k^q \, O_k^q(S_x, S_y, S_z) \qquad (8)$$

where the electronic g-matrix may be replaced by an isotropic value of $g_{iso}^{Fe^{3+}} = 2.002$, β_e denotes the Bohr magneton, $\mathbf{B}_0$ the external magnetic field, B_k^q are the FS spin-Hamiltonian parameters, and O_k^q are the extended Stevens spin operators.[31] In principle, all conceivable B_k^q parameters, resulting from 2nd to 4th-(Fe^{3+}) tensors, have to be considered. However, experimentally only the 2nd-rank B_2^q parameters for Fe^{3+} could reliably be determined by means of numerical spectrum simulation[30] using Eq. (8).

3. Results and discussion

In order to verify the formation of the expected tetragonal $PbTiO_3$ perovskite phase after calcination, XRD data of the CPP precursor and the resulting $PbTiO_3$ nanopowder after calcination at 800 °C are shown in Fig. 2. Whereas the XRD pattern of the precursor shows no significant peaks, indicating the expected amorphous structure, the XRD pattern of a calcined sample exhibits the pattern expected for tetragonal $PbTiO_3$ powder with the corresponding Bragg reflections indexed.

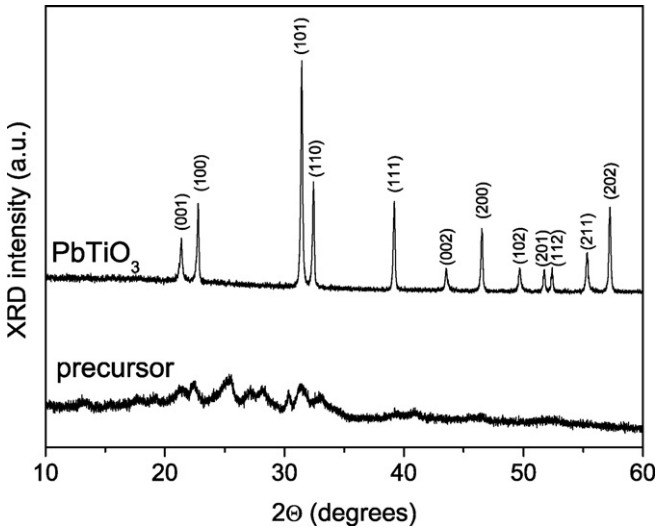

Fig. 2. Powder diagram of a $PbTiO_3$ sample prepared by the combined polymerization and pyrolysis (CPP) route and calcined at 800 ° C (top) in comparison with that of the precursor (bottom). The indexed reflections indicate the formation of single-phase tetragonal $PbTiO_3$.

By subsequently using Raman spectroscopy it is possible to account for the expected soft-mode behavior of ferroelectric $PbTiO_3$ particles. The soft mode E(1TO) is a prerequisite for the existence of long-range phenomena and often is used as a fingerprint for the existence of ferroelectricity. The corresponding spectra are displayed in Fig. 3. For a sample calcined at 800 °C, all expected Raman-active modes for $PbTiO_3$[29] were observed. As compared to the Raman frequencies reported for

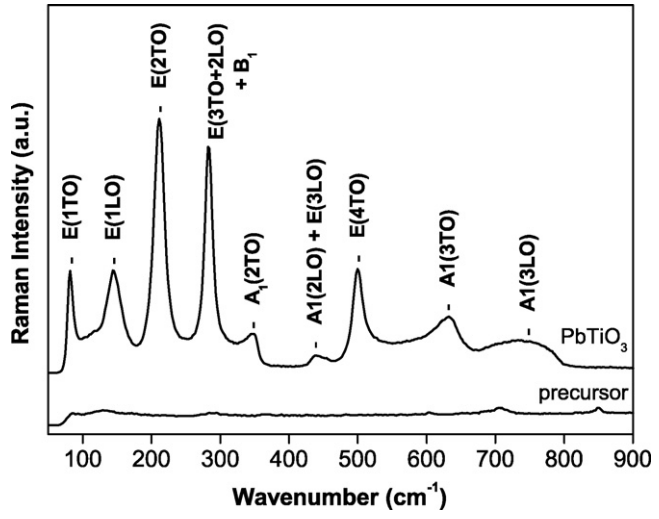

Fig. 3. Comparison of the Raman spectrum of a powdered $PbTiO_3$ sample synthesized via combined polymerization and pyrolysis (CPP) route and calcined at 800 °C (top) with that of the precursor (bottom). All Raman modes expected for $PbTiO_3$ could be observed and assigned.

'pure' $PbTiO_3$ no significant shifts could be registered for the Fe^{3+}-modified $PbTiO_3$ compounds. On the other hand, for the amorphous precursor no significant Raman-active modes could be detected.

The '*method-of-choice*' for the characterization of prevailing defect structure in the nanoparticles with respect to the formation of $(Fe'_{Ti}-V_O^{\bullet\bullet})^{\bullet}$ defect dipoles, as well as its orientation as a function of $PbTiO_3$ mean grain size is electron paramagnetic resonance (EPR) spectroscopy.[9,10] The information content obtained from the analysis of the EPR spectra is twofold. First, it can be distinguished between 'isolated' Fe'_{Ti} functional centers and centers that have formed a $(Fe'_{Ti}-V_O^{\bullet\bullet})^{\bullet}$ defect dipole for reasons of charge compensation. Second, the site symmetry at the Fe^{3+}-site is obtained, for which reason in case of a $(Fe'_{Ti}-V_O^{\bullet\bullet})^{\bullet}$ defect dipole, its orientation with respect to the orientation of the spontaneous polarization may be deduced.[19] Correspondingly, the defect dipoles may be oriented either parallel $(Fe'_{Ti}-V_O^{\bullet\bullet})^{\bullet}_{||}$ or perpendicular $(Fe'_{Ti}-V_O^{\bullet\bullet})^{\bullet}_{\perp}$ with respect to the orientation of P_S. In case of an 'isolated' Fe'_{Ti} center, an isotropic EPR line accounts for a cubic and paraelectric $PbTiO_3$ phase.

The corresponding EPR spectra for the obtained Fe^{3+}-modified $PbTiO_3$ nanopowders with varying mean grain size are given in Fig. 4. For comparison, also the EPR spectrum of a 'bulk' sample with mean grain size of 500 nm is depicted (top). The spectrum consists of a dominant low-field peak at ≈ 100 mT characteristic for the existence of $(Fe'_{Ti}-V_O^{\bullet\bullet})^{\bullet}_{||}$ defect dipoles.[28] For reduced grain size, additional peaks occur in the EPR spectra (center, bottom). These may be explained by the following scenario. For nano-sized samples an increasing contribution arises from the surface of the nanograins. According to a *core–shell model*,[32,22] this surface has cubic $PbTiO_3$ structure and thus is paraelectric. In cubic crystal symmetry, the advantage in energy of formation of an $(Fe'_{Ti}-V_O^{\bullet\bullet})^{\bullet}$ defect associate over the 'isolated' defects (Fe'_{Ti}, $V_O^{\bullet\bullet}$) [11] vanishes. Consequently,

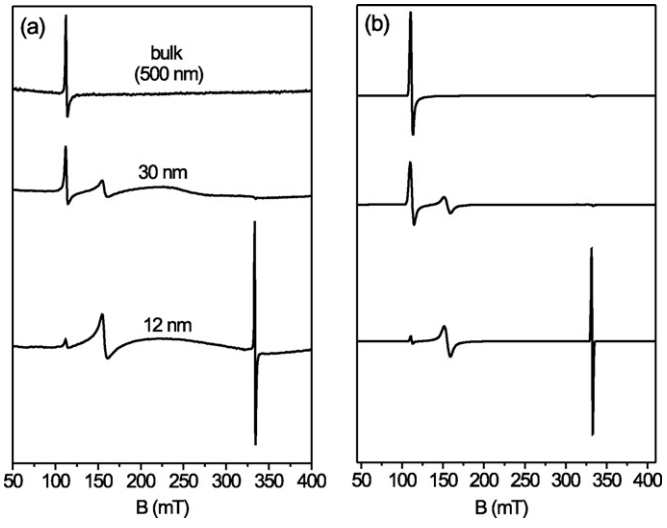

Fig. 4. Room-temperature X-band (9.5 GHz) EPR spectra of Fe^{3+}-modified $PbTiO_3$ nanopowders with varying mean grain size. (a) Experiment and (b) numerical simulation.

the observation of an isotropic EPR at $g = 2.002$ (Fig. 4, bottom) accounts for the existence of an isolated Fe'_{Ti} center in a paraelectric surface region. The third resonance at ≈150 mT is characteristic for a $(Fe'_{Ti}-V_O^{\bullet\bullet})^{\bullet}$ defect dipole of rhombic site symmetry at the site of the Fe^{3+} functional center. Its origin may be twofold. First, it may be a $(Fe'_{Ti}-V_O^{\bullet\bullet})^{\bullet}_{\perp}$ defect dipole. Second, it may be a $(Fe'_{Ti} - V_O^{\bullet\bullet})^{\bullet}$ defect dipole in a distorted crystal symmetry. Both scenarios agree with the existence of a distorted interface layer in the nanocrystals between the ferroelectric core and the paraelectric surface.

However, the present results do not allow to monitor the complete size-driven phase transition, for which exclusively 'cubic' EPR spectra are expected. Consequently, only an upper limit for the corresponding critical size $d_{crit} < 12$ nm can be given.

The obtained EPR spectra may nicely be reproduced by means of numerical spectrum simulation [30] by assuming a superposition of three different centers with axial, rhombic and cubic site symmetries (cf. Fig. 4(b)). The broad line occurring only in the spectra of the nano-sized compounds (30 and 12 nm) between 150 and 270 mT is due to the iron oxide (Fe_2O_3) on the surface of the nanograins and was not considered in the spectrum simulations.

4. Conclusion and outlook

In summary, the synthesis of Fe^{3+}-modified $PbTiO_3$nanopowders has been reported by using the CPP route. The EPR results clearly indicate marked size effects by approaching to the critical grain size ($d_{crit} < 12$ nm) at which a size-driven tetragonal-to-cubic phase transition is observed at room temperature. The obtained results agree well with the proposed *core–shell model* [32,22] and are a superposition of three phases corresponding to a ferroelectric core (tetragonal), a distorted interface layer (rhombic) and a paraelectric shell (cubic). The Fe^{3+}-modified $PbTiO_3$ nanoparticles thus consist of a ferroelectric core, and a cubic dead layer which is paraelectric. These results are also consistent with the recent Landau phenomenological theory calculations for confined ferroelectric nanoparticles.[33]

In order to enlighten the interplay between nano-structuring and defect structure in more detail, the existing set of samples has to be extended. In particular, by soft-milling compounds with mean grain sizes below the critical grain size d_{crit} shall be obtained. Furthermore, we aim to investigate the size-driven phase transition and accurately determine the critical grain size d_{crit}. Future work will be the detailed extension of structural characterisation by using mainly multi-frequency high-field EPR and the standard methods such as XRD, Raman and dielectric spectroscopy. Particularly, in the content of size effects, the soft mode reduction, change of T_C and softening of dielectric permittivity curves are the important open questions to be considered. Multi-frequency high-filed EPR (Q-band (35 GHz), W-band (95 GHz) and higher frequencies) have the advantage to detect the higher Fe^{3+} energy transitions. So that, we can have more information about the sign and the size dependency of the zero field splitting parameter.

Acknowledgments

We are grateful to Klaus Seifert, Prof. Dr. Jürgen Rödel as well as Dr. P. Jakes for assistance in the synthesis of the nanocrystals. This research has been financially supported by the DFG centre of excellence 595 '*Electrical Fatigue in Functional Materials*'. E.E. is grateful for support from COST 539 program and K.K. is grateful to a grant from TUBITAK (BiDEB-2228).

References

[1]. Scott, J. F., The physics of ferroelectric ceramics thin films for memory applications. *Ferroelectr. Rev.*, 1998, **1**, 1–129.
[2]. Ishikawa, K., Yoshikawa, K. and Okada, N., Size effect on the ferroelectric phase transition in $PbTiO_3$ ultrafine particles. *Phys. Rev. B*, 1988, **37**, 5852–5855.
[3]. Ishikawa, K., Okada, N., Takada, K., Nomura, T., Hagino, M. and Toyoda, K., Initial stage of growth process of lead titanate fine particles. *Jpn. J. Appl. Phys.*, 1994, **33**, 5412–5415.
[4]. Ishikawa, K., Nomura, T., Okada, N. and Takada, K., Size effect on the phase transition in $PbTiO_3$ fine particles. *Jpn. J. Appl. Phys.*, 1996, **35**, 5196–5198.
[5]. Chattopadhyay, S., Ayyub, P., Palkar, V. R. and Multani, M., Size-induced diffuse phase transition in the nanocrystalline ferroelectric $PbTiO_3$. *Phys. Rev. B*, 1995, **52**, 13177–13183.
[6]. Junquera, J. and Ghosez, P., Critical thickness for ferroelectricity in perovskite ultrathin films. *Nature*, 2003, **422**, 506–509.
[7]. Ahn, C. H., Triscone, J. M. and Mannhart, J., Electric field effect in correlated oxide systems. *Nature*, 2003, **424**, 1015–1018.
[8]. Chandra, P., Dawber, M., Littlewood, P. B. and Scott, J. F., Scaling of coercive field with thickness in thin-film ferroelectrics. *Ferroelectrics*, 2004, **313**, 7–13.
[9]. Eichel, R-A., Defect structure of oxide ferroelectrics-valence state, site of incorporation, mechanisms of charge compensation and internal bias fields. *J. Electroceram.*, 2007, **19**, 9–21.
[10]. Eichel, R.-A., Characterization of defect structure in acceptor-modified piezoelectric ceramics by multifrequency and multipulse electron paramagnetic resonance spectroscopy. *J. Am. Ceram. Soc.*, 2008, **91**, 691–701.
[11]. Meštrić, H., Eichel, R-A., Kloss, T., Dinse, K-P., Laubach, So., Laubach, St. and Schmidt, P. C., Iron-oxygen vacancy defect centers in $PbTiO_3$: Newman superposition model analysis and density functional calculations. *Phys. Rev. B*, 2005, **71**, 134109.
[12]. Meštrić, H., Eichel, R-A., Dinse, K-P., Ozarowski, A., van Tol, J., Brunel, L. C., Kungl, H., Hoffmann, M. J., Schönau, K. A., Knapp, M. and Fuess, H., Iron-oxygen vacancy defect association in polycrystalline iron-modified $PbZrO_3$ antiferroelectrics: multifrequency electron paramagnetic resonance and Newman superposition model analysis. *Phys. Rev. B*, 2006, **73**, 184105.
[13]. Eichel, R-A., Dinse, K-P., Kungl, H., Hoffmann, M. J., Ozarowski, A., van Tol, J. and Brunel, L. C., Exploring the morphotropic phase boundary in copper(II)-modifed $Pb[Zr_{0.54}Ti_{0.46}]O_3$ ferroelectrics. *Appl. Phys. A*, 2005, **80**, 51–54.
[14]. Eichel, R.-A., Erhart, P., Träskelin, P., Albe, K., Kungl, H. and Hoffmann, M. J., Defect-dipole formation in copper-doped $PbTiO_3$ ferroelectrics. *Phys. Rev. Lett.*, 2008, **100**, 095504.
[15]. Kleebe, H-J., Lauterbach, S., Silvestroni, L., Kungl, H., Hoffmann, M. J., Erdem, E. and Eichel, R-A., Formation of magnetic grains in ferroelectric $Pb[Zr_{0.6}Ti_{0.4}]O_3$ ceramics doped with Fe^{3+} above the solubility limit. *Appl. Phys. Lett.*, 2009, **94**, 142901.
[16]. Eichel, R-A., Meštrić, H., Kungl, H. and Hoffmann, M. J., Multi-frequency electron paramagnetic resonance analysis of polycrystalline gadolinium-doped $PbTiO_3$—charge compensation and site of incorporation. *Appl. Phys. Lett.*, 2006, **88**(1–3), 122506.
[17]. Erdem, E., Eichel, R-A., Kungl, H., Hoffmann, M. J., Ozarowski, A., van Tol, H. and Brunel, L. C., Characterization of $(Fe'_{Zr,Ti} - V_O^{\bullet\bullet})^{\bullet}$ defect dipoles in (La,Fe)-codoped PZT 52.5/47.5 piezoelectric ceramics by multifrequency electron paramagnetic resonance spectroscopy. *IEEE Trans. UFFC*, 2008, **55**, 1061–1068.
[18]. Erdem, E., Drahus, M. D., Eichel, R-A., Kungl, H., Hoffmann, M. J., Ozarowski, A., van Tol, H. and Brunel, L. C., Defect structure in 'soft' (Gd,Fe)-codoped PZT 52.5/47.5 piezoelectric ceramics. *Funct. Mater. Lett.*, 2008, **1**, 7–11.
[19]. Erdem, E., Eichel, R-A., Kungl, H., Hoffmann, M. J., Ozarowski, A., van Tol, H. and Brunel, L. C., Local symmetry-reduction in tetragonal (La,Fe)-codoped $Pb[Zr_{0.4}Ti_{0.6}]O_3$ piezoelectric ceramics. *Phys. Scr.*, 2007, **T129**, 12–16.
[20]. Zhang, L. X., Erdem, E., Ren, X. and Eichel, R-A., Reorientation of $(Mn_{Ti}{-}V_O^{\bullet\bullet})^{\times}$ defect dipoles in acceptor-modified $BaTiO_3$ single crystals—an electron paramagnetic resonance study. *Appl. Phys. Lett.*, 2008, **93**, 202901.
[21]. Jaffe, B., Cook, W. R. and Jaffe, H., *Piezoelectric Ceramics*. Academic Press Limited, Bedford, OH, 1971.
[22]. Erdem, E., Semmelhack, H-C., Böttcher, R., Rumpf, H., Banys, J., Matthes, A., Gläsel, H-J., Hirsch, D. and Hartmann, E., Study of the tetragonal-to-cubic phase transition in $PbTiO_3$ nanopowders. *J. Phys. Condens. Mater.*, 2006, **18**, 3861–3874.
[23]. Erdem, E., Böttcher, R., Semmelhack, H-C., Gläsel, H-J., Hartmann, E. and Hirsch, D., Preparation of lead titanate ultrafine powders from combined polymerisation and pyrolysis route. *J. Mater. Sci.*, 2003, **38**, 3211–3217.
[24]. Böttcher, R., Klimm, C., Michel, D., Semmelhack, H-C., Völkel, G., Gläsel, H-J. and Hartmann, E., *Phys. Rev. B*, 2000, **62**, 2085.
[25]. Erdem, E., Böttcher, R., Semmelhack, H-C., Gläsel, H-J. and Hartmann, E., Multi-frequency EPR studyof Cr^{3+} doped lead titanate ($PbTiO_3$) nanopowders. *Phys. Status Solidi (b)*, 2003, **239**, 7–9.
[26]. Rozenberg, A. S., Aleksandrova, E. I., Dzardimalieva, G. I. and Pomagailo, A. D., Preparation and reactivity of metal-containing monomers. *Russ. Chem. Bull.*, 1995, **44**, 858–866.
[27]. Erdem, E., Matthes, A., Böttcher, R., Gläsel, H-J. and Hartmann, E., Size effects in ferroelectric $PbTiO_3$ nanomaterials observed by multi-frequency electron paramagnetic resonance spectroscopy. *J. Nanosci. Nanotechnol.*, 2008, **8**, 702–716.
[28]. Meštrić, H., Eichel, R-A., Dinse, K-P., Ozarowski, A., van Tol, J. and Brunel, L. C., High-frequency electron paramagnetic resonance investigation of the Fe^{3+} impurity center in polycrystalline $PbTiO_3$ in its ferroelectric phase. *J. Appl. Phys.*, 2004, **96**, 7440–7444.
[29]. Burns, G. and Scott, B. A., Lattice modes in ferroelectric perovskites: $PbTiO_3$. *Phys. Rev. B*, 1973, **7**, 3088–3101.
[30]. Stoll, S. and Schweiger, A., EasySpin, a comprehensive software package for spectral simulation and analysis in EPR. *J. Magn. Reson.*, 2006, **178**, 42–55.
[31]. Abragam, A. and Bleaney, B., *Electron Paramagnetic Resonance of Transition Ions*. Clarendon Press, Oxford, 1970.
[32]. Aoyagi, S., Kuroiwa, Y., Sawada, A., Kawaji, H. and Atake, T., Size effect on crystal structure and chemical bonding nature in $BaTiO_3$ nanopowder. *Journal Thermal Analy Cal*, 2005, **81**, 627–630.
[33]. Morozovska, A. N., Glinchuk, M. D. and Eliseev, E. A., Phase transitions induced by confinement of ferroic nanoparticles. *Phys. Rev. B*, 2007, **76**(1–13), 014102.